JMEPEG (1999) 8:429-436

Ultrasonic Measurements of Stiffness in Thermal-Mechanically Fatigued IM7/5260 Composites

M.D. Seale and E.I. Madaras

(Submitted 16 March 1999; in revised form 1 April 1999)

In recent years, ultrasonic methods have been developed that can measure the mechanical stiffness of composites. The Lamb wave velocity is directly related to the material parameters, so an effective method exists to ascertain the stiffness of composites by measuring the velocity of these waves. In this study, a Lamb wave measurement system was used to measure the bending and out-of-plane stiffness coefficients of thermoset composite laminates undergoing thermal-mechanical loading. A series of 16 ply and 32 ply composite laminates were subjected to thermal-mechanical fatigue (TMF) in load frames equipped with special environmental chambers. The composite system studied was a graphite fiber-reinforced bismaleimide thermoset, IM7/5260. The samples were subjected to both high and low temperature profiles as well as high-strain and low-strain profiles. The bending and out-of-plane stiffnesses for composite samples that have undergone over 6000 cycles of combined thermal and mechanical fatigue are reported. The Lamb wave generated elastic stiffness results have shown decreases of up to 64% at 4706 cycles for samples subjected to TMF at high temperatures and less than a 10% decrease at over 6000 cycles for samples subjected to TMF at low temperatures.

Keywords aging, Lamb wave, nondestructive, thermal-mechanical, thermoset, ultrasonic

1. Introduction

Composite materials are being widely used today by aerospace, automotive, and a number of other commercial industries because of their advantages over conventional metals. They have a high strength-to-weight ratio and can be constructed to meet specific design needs. Composites that will be used in the next generation of aerospace structures will be required to operate under severe thermal and mechanical loading environments. Subjecting these materials to such conditions can cause reductions in their load carrying capabilities, which could compromise safety. With this in mind, considerable attention has been given to understanding how composites respond to various forms of damage.

One degradation mechanism in composites that has received much consideration is mechanical fatigue. O'Brien et al. (Ref 1) and Charewicz and Daniel (Ref 2) have examined the fatigue behavior of laminates and proposed lifetime prediction models based on fatigue factors such as increased matrix cracking, delamination growth, and stiffness loss. Ogin et al. (Ref 3, 4) and Lim and Hong (Ref 5) have modeled the stiffness reduction in composites due to the effects of matrix cracking. Laws and Dvorak (Ref 6) have investigated the progression of matrix cracking as well as stiffness loss due to transverse cracking.

In addition to fatigue, thermal degradation of composites has also received much attention. Street et al. (Ref 7) investigated the response of AS/3501-6 composites to elevated temperatures by measuring interlaminar fracture toughness, interlaminar shear strength, and hardness. Deterioration of the matrix was found to be the primary degradation mechanism. Herakovich and Hyer (Ref 8) measured the crack density as a function of cycles for thermally cycled graphite/epoxy composites. The main cause of material degradation was found to be transverse matrix cracking. Henaff-Gardin et al. (Ref 9) used x-ray radiography to observe cracking in T300/914 composites that were subjected to cyclic thermal loading. The crack density was observed to increase with the number of thermal cycles. Tao et al. (Ref 10) measured interlaminar shear strength and fracture toughness in an effort to monitor the effects of thermal as well as thermal and mechanical fatigue in IM7/K3B laminates. Both measurement methods were found to yield similar results.

Under general thermal-mechanical loading, both fatigue damage and thermal degradation of composites can occur. With the increased use of advanced materials in aerospace vehicles, techniques are required to nondestructively evaluate the structural integrity of composites that are subjected to thermal-mechanical fatigue (TMF). Among the various techniques available, ultrasonic Lamb waves offer a useful method of evaluating these composite materials. Studies have been conducted that show a reduction in Lamb wave velocity due to a loss of stiffness caused by matrix cracking (Ref 11-14). Inversion techniques have even been used by Karim et al. (Ref 15) and Mal et al. (Ref 16) to determine the material parameters of composites from experimental Lamb wave data. Recently, Shih et al. (Ref 17) have used Lamb wave measurements to determine stiffness constants in fatigued composites.

Although studies have been conducted using Lamb waves to examine fatigue damage (Ref 11-14, 17), few studies that use ultrasonic nondestructive evaluation (NDE) techniques to monitor either thermal degradation or TMF in polymer matrix composites have been done. However, ultrasonic Lamb waves have been shown by Seale et al. (Ref 11) and Bar-Cohen et al.

M.D. Seale, National Research Council Associate, and **E.I. Madaras,** NASA Langley Research Center, Mail Stop 231, Hampton, VA, 23681, USA. Contact e-mail: m.d.seale@larc.nasa.gov.

(Ref 18) to be an effective method for characterizing thermal damage in AS4/977-3 and AS4/3501-6 composites, respectively. This study explores the use of Lamb waves to monitor the effects of TMF in thermoset composite specimens. A Lamb wave scanning system was used to measure stiffness values on thermal-mechanically fatigued composites. The results for samples that have been subjected to over 6000 TMF cycles are discussed.

2. Samples and TMF Process

The composite material studied was a graphite fiber reinforced bismaleimide thermoset, IM7/5260. The 122 by 30.5 cm samples were manufactured with 16 and 32 plies and had stacking sequences of $[45/0/–45/90]_{2S}$ and $[45/0/–45/90]_{4S}$, respectively, and nominal thicknesses of 0.248 and 0.483 cm, respectively. The samples were subjected to TMF in either 98 or 222 kN (22 or 50 kip) capacity load frames equipped with environmental chambers that had a usable temperature range of –54 to +344 °C. The chamber dimensions were 40 cm wide by 67 cm tall by 40 cm deep, and the grips for the load frames were located outside of the chambers. The upper and lower portions of the samples remained outside of the chambers, so only the middle 67 cm sections along the length of the samples were exposed to thermal extremes.

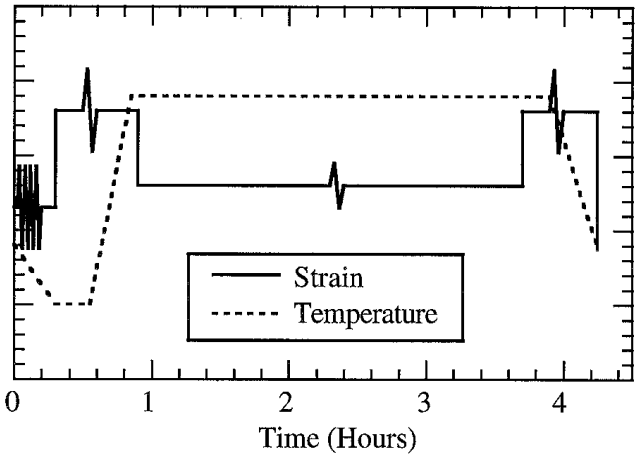

Fig. 1 Thermal-mechanical fatigue profile

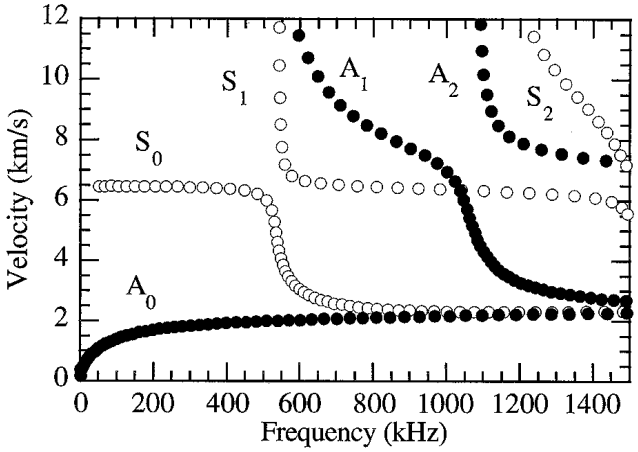

Fig. 2 Lamb wave dispersion curve for composite samples. The symmetric modes are indicated by open circles, and the antisymmetric modes are indicated by solid circles.

Each TMF cycle lasted for 255 min. The profile used for this study is shown in Fig. 1. Since both high and low strain profiles as well as high-temperature and low-temperature profiles were used for the various samples, the units for strain and temperature have been omitted from the figure. The load was applied in the 0° direction (along the length of the specimens). The strain levels for the low-strain profiles ranged from 0 to 2000 με with a strain at or above 1040 με for 180 min. The strain levels for the high-strain profiles ranged from 0 to 3000 με with a strain at or above 1560 με for 180 min. The temperature extremes for the high-temperature cycling were chosen to be –18 and +177 °C with a sustained temperature of +177 °C for 180 min. The temperature extremes for the low-temperature cycling were chosen to be –18 and +135 °C with a sustained temperature of +135 °C for 180 min. The 16 ply samples were subjected to low-strain levels and both high-temperature and low-temperature profiles. The 32 ply samples were exposed to low-temperature and high-strain profiles only.

3. Lamb Waves and Laminated Plate Theory

The Lamb wave dispersion curve for the samples used in this study is shown (Fig. 2). As can be seen from the figure, two classes of Lamb mode solutions exist. The modes are defined as symmetric, S_n, or antisymmetric, A_n, based on the symmetry of the displacement of the plate with respect to the midplane. At frequencies below 500 kHz, only the lowest order symmetric mode, S_0, and lowest order antisymmetric mode, A_0, propagate. In this region, the S_0 or extensional plate mode is almost nondispersive, and the A_0 or flexural plate mode is highly dispersive. Also, the flexural mode velocity approaches zero as the frequency approaches zero. At higher frequencies, additional modes begin to propagate. This study investigates solutions for the flexural mode.

Consider a unidirectional lamina to be under a condition of plane stress. With the *x*-axis defined as in the fiber direction, the *y*-axis transverse to the fibers, and the *z*-axis being out of the plane of the plate, the stress-strain relationship along the material axes is given by the following:

$$\begin{bmatrix} \sigma_1 \\ \sigma_2 \\ \tau_4 \\ \tau_5 \\ \tau_6 \end{bmatrix} = \begin{bmatrix} Q_{11} & Q_{12} & 0 & 0 & 0 \\ Q_{12} & Q_{22} & 0 & 0 & 0 \\ 0 & 0 & Q_{44} & 0 & 0 \\ 0 & 0 & 0 & Q_{55} & 0 \\ 0 & 0 & 0 & 0 & Q_{66} \end{bmatrix} \begin{bmatrix} \varepsilon_1 \\ \varepsilon_2 \\ \gamma_4 \\ \gamma_5 \\ \gamma_6 \end{bmatrix} \quad \text{(Eq 1)}$$

where abbreviated subscript notation has been used. The subscripts 1, 2, 4, 5, and 6 represent the *xx*, *yy*, *yz*, *xz*, and *xy* components, respectively. The normal and shear stresses are given by σ and τ, respectively, and the normal and shear strains are given by ε and γ, respectively. The Q_{ij} for $i, j = 1, 2, 6$ are the plane-stress stiffness components, and for $i, j = 4, 5$ they represent the

shear stiffness components. The bending stiffnesses, D_{ij}, and the out-of-plane stiffnesses, A_{jj}, are obtained by integrating the Q_{ij} through the thickness of the plate. For each lamina, the Q_{ij} must be rotated according to the orientation of each ply with respect to the wave propagation direction. The bending and out-of-plane stiffnesses are defined as the following (Ref 19):

$$D_{ij} = \int_{-h/2}^{h/2} (Q'_{ij})_k \, z^2 \, dz \qquad i,j = 1, 2, 6 \tag{Eq 2}$$

and

$$A_{jj} = k_j^2 \int_{-h/2}^{h/2} (Q'_{jj})_k \, dz \qquad j = 4, 5 \tag{Eq 3}$$

where the subscript k represents each layer in the laminate, k_j is a shear correction factor, and h is the total thickness of the plate. The Q'_{ij} are the transformed stiffness coefficients, which take into account the ply orientation.

For waves propagating in the 0° direction in a symmetric quasi-isotropic plate, the dispersion relation for the flexural mode is given by the following (Ref 19):

$$(D_{11}k^2 + A_{55} - I\omega^2)(D_{66}k^2 + A_{44} - I\omega^2)(A_{55}k^2 - \rho^*\omega^2) - (D_{16}k^2)^2(A_{55}k^2 - \rho^*\omega^2) - (A_{55}k)^2(D_{66}k^2 + A_{44} - I\omega^2) = 0 \tag{Eq 4}$$

For waves propagating in the 90° direction, the relation is the following (Ref 19):

$$(D_{22}k^2 + A_{44} - I\omega^2)(D_{66}k^2 + A_{55} - I\omega^2)(A_{44}k^2 - \rho^*\omega^2) - (D_{16}k^2)^2(A_{44}k^2 - \rho^*\omega^2) - (A_{44}k)^2(D_{66}k^2 + A_{55} - I\omega^2) = 0 \tag{Eq 5}$$

In the equations, ω is the angular frequency and k is the wave number. I and ρ^* are defined as the following (Ref 20):

$$I = \int_{-h/2}^{h/2} \rho \, dz \tag{Eq 6}$$

and

$$\rho^* = \int_{-h/2}^{h/2} \rho z^2 dz \tag{Eq 7}$$

where ρ is the density and h is the plate thickness. Although multiple roots exist for the dispersion relations, only the roots in Eq 4 and 5 that satisfy the condition that the velocity approaches zero as the frequency approaches zero are the ones corresponding to the flexural plate mode (Fig. 2). Once ω and k are known, the velocity is found from the following:

$$v = \frac{\omega}{k} \tag{Eq 8}$$

The Lamb wave dispersion curve is obtained by plotting the velocity as a function of the frequency.

The effects of altering the A_{44}, A_{55}, D_{11}, D_{16}, and D_{66} stiffnesses on the flexural dispersion relation given by Eq 4 are shown in Fig. 3. Decreasing the values of D_{16}, D_{66}, and A_{44} by 25% did not significantly alter the dispersion curve. The effects of altering these three parameters is shown in Fig. 4. In Fig. 3, it is observed that decreasing A_{55} by 25% alters the curve more substantially than decreasing D_{11} by 25%.

Figure 4 shows a plot of the percent change in velocity as a function of frequency for 25% reductions in each of the five stiffness values. The stiffnesses D_{11} and A_{55} are the only constants that change the velocity by more than 0.5%. Also, D_{11} has a greater effect on the velocity at lower frequencies, and A_{55} controls the behavior of the dispersion curve at higher frequencies.

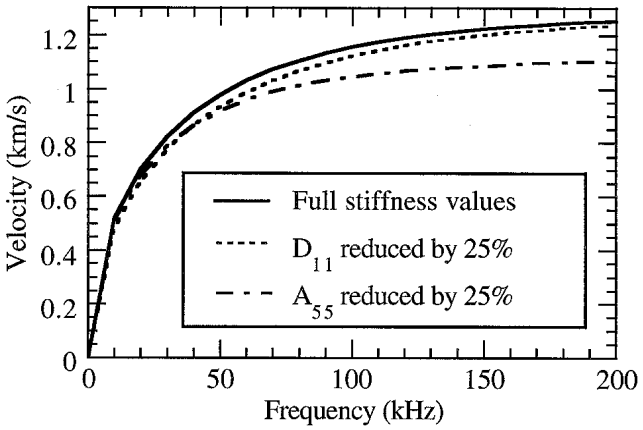

Fig. 3 Flexural dispersion curves using full values of D_{11}, D_{16}, D_{66}, A_{44}, and A_{55}, with D_{11} reduced by 25%, and with A_{55} reduced by 25%. The curves with values of D_{16}, D_{66}, and A_{44} reduced by 25% could not be discerned from the curve constructed using the full stiffness values.

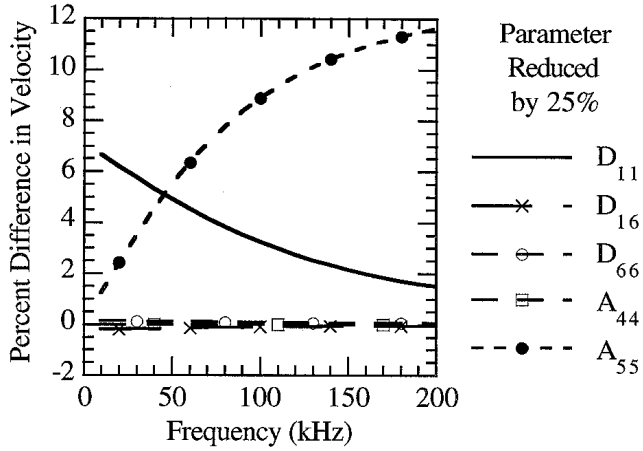

Fig. 4 Plot of the percent reduction in velocity as a function of frequency for a 25% decrease in each of the stiffness constants

Since D_{11} and A_{55} are the only constants affecting the curve, only these two parameters were adjusted to fit the experimental data. The values of D_{16}, D_{66}, and A_{44} were fixed at the theoretical values obtained from Eq 2 and 3. The dispersion curve for propagation in the 90° direction, given by Eq 5, is the same as that shown in Fig. 3, except the constants controlling the behavior are D_{22} and A_{44}. For propagation in the 90° direction, the values of D_{16}, D_{66}, and A_{55} do not affect the dispersion curve and were held constant. Only the values of D_{22} and A_{44} were used to fit the experimental data.

4. Lamb Wave Measurements

In this measurement, two transducers were used in a pulse/receive arrangement to determine the velocity of the flexural plate mode over a wide frequency range. The receiving sensor was moved by small increments in order to assure that the same peak in the waveform was followed over the total separation distance. The velocity at each frequency was calculated from the known transducer separation and the measured time-of-flight. Using this measurement system, the velocity measurements have been shown to be accurate and repeatable to within 1% resulting in reconstructed stiffness values repeatable to within 4% (Ref 21).

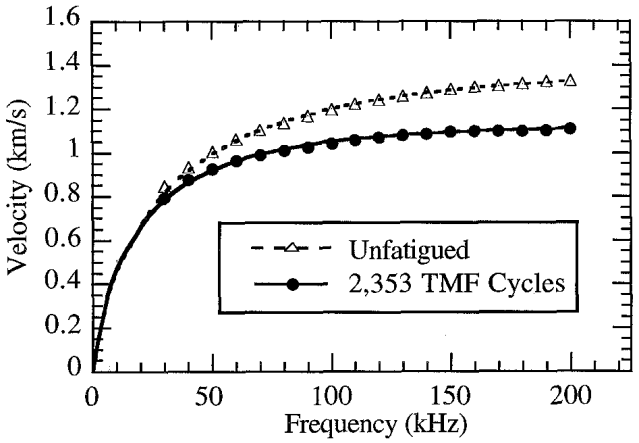

Fig. 5 Experimental dispersion curves for an unfatigued sample and for one with 2353 TMF cycles at a low strain/high temperature profile. Also shown are the reconstructed dispersion curves for each of the samples.

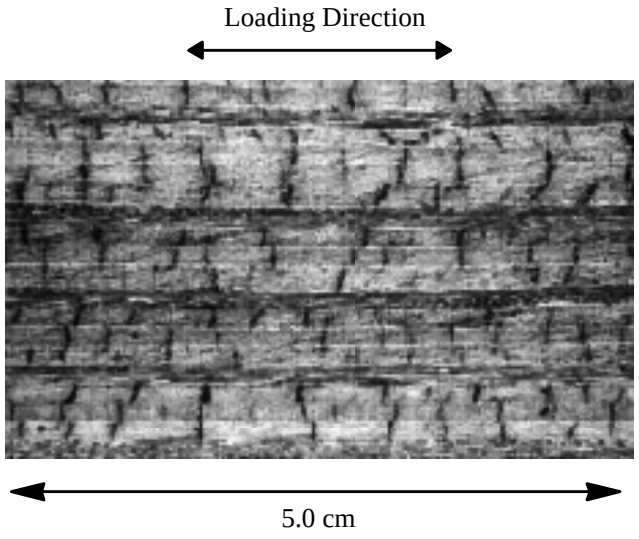

Fig. 6 Micrograph of a sample subjected to TMF at low strains and low temperatures

Once the velocity as a function of frequency was obtained, the bending and out-of-plane shear stiffnesses were computed from a reconstruction of the flexural dispersion curve that best fit the data. The D_{11} and A_{55} stiffness matrix components were determined from velocity measurements in the 0° direction, and the values of D_{22} and A_{44} were obtained from measurements in the 90° direction. A mechanical scanner was used to move the sensors over the surface to map the time-of-flight, velocity, and stiffness of the entire specimen. Access to only one side of the material was required, and no couplants were required because the sensors are dry coupled to the surface of the plate.

The Lamb wave scanning system was used to measure the stiffness in the 0 and 90° directions on unfatigued specimens as well as on samples subjected to TMF. The sensor separation was varied from 2.75 to 4.75 cm in increments of 0.4 cm. An eight-cycle Gaussian-enveloped sine wave was used to generate the signal, and the received signal was sampled at 25 MHz. The frequency was swept in 10 kHz steps from 30 to 200 kHz, and the velocity at each frequency was obtained. The thicknesses of the respective samples were given above, and the density, estimated from common values for polymer matrix composites, was taken to be 1560 kg/m^3. From the data for the 0° measurements, values for the out-of-plane shear stiffness, A_{55}, and bending stiffness, D_{11}, were calculated by adjusting these parameters in Eq 4 in order to produce the best fit to the experimental velocity measurements. In a similar manner, the stiffnesses A_{44} and D_{22} were obtained by adjusting these parameters in Eq 5 in order to produce the best fit to experimental velocity measurements in the 90° direction.

Shown in Fig. 5 is the average of ten experimental velocity measurements in the 0° direction for an unfatigued sample and for one with 2353 cycles of TMF at low-strain levels and high-temperature extremes. In the figure, error bars representing the standard deviation in velocity at each frequency were on the order of the size of the symbols. Also shown are the reconstructed dispersion curves that were obtained by altering A_{55} and D_{11} to best fit the experimental data. For the curves shown, the value of A_{55} decreased by 34%, and the value of D_{11} increased by 2% for the sample subjected to TMF as compared to the unfatigued sample.

Shown in Fig. 6 is a micrograph of the edge of a sample subjected to TMF that shows matrix cracking. Previous strain gage measurements show that matrix cracking due to fatigue damage in composites leads to a decrease in elastic moduli (Ref 11). Since the out-of-plane shear carrying capabilities of the composite are matrix dominated, the decrease in the stiffness A_{55} due to matrix cracking was as expected.

The stiffness D_{11} is controlled by the fibers if the bending occurs in the fiber direction and by the matrix if the bending occurs perpendicular to the fibers. Because fiber damage is

probably not occurring in the samples, the value of D_{11} would only be influenced by the matrix cracking. Due to the fact that a quasi-isotropic architecture was used, a smaller decrease in D_{11} would be expected. Although a decrease in the value of D_{11} with TMF was anticipated, an insignificant increase was observed. This was most likely due to the insensitivity of the dispersion curve to changes in bending stiffness over the measurement frequency range (30 to 200 kHz). In this region, the parameter dominating the behavior of the curve will be A_{55} (see Fig. 4). Only a few data points exist at frequencies below 50 kHz where D_{11} controls the behavior of the curve. Due to this lack of data, the constant D_{11} will not be as accurate as the constant A_{55}. Similarly, for propagation in the 90° direction, the constant A_{44} will be more accurate than the constant D_{22}.

Stiffness mappings for a variety of samples were made in situ as well as with the specimens removed from the environmental chambers. With the samples out of the chambers, a stiffness mapping of 75 different regions along the entire length of the panel could be obtained. Due to the constraints of the environmental chambers, only 20 stiffness values in the middle of the specimens could be obtained for the in situ measurements. Mappings of A_{55} and D_{11} were acquired from velocity measurements along the length of the samples. Similarly, mappings of A_{44} and D_{22} were acquired from velocity measurements across the width of the samples.

Sample results of stiffness mappings of A_{55} are shown in Fig. 7 for three of the composites. In the figure, the stiffnesses have been normalized to the average stiffness measured for the unfatigued sample. Stiffness results were also obtained for values of A_{44} from measurements in the 90° direction. The results of these scans are shown in Fig. 8. As with the A_{55} measurements, the stiffnesses have been normalized to the average stiffness obtained for the unfatigued specimen. The higher stiffness values observed in the regions at the top and bottom of the specimens that were subjected to TMF were due to that portion of the sample being out of the environmental chambers and, therefore, not exposed to the same TMF process as the rest of the sample. The average normalized stiffnesses as well as standard deviations for the samples exposed to low and high strain levels are shown in Tables 1 and 2, respectively.

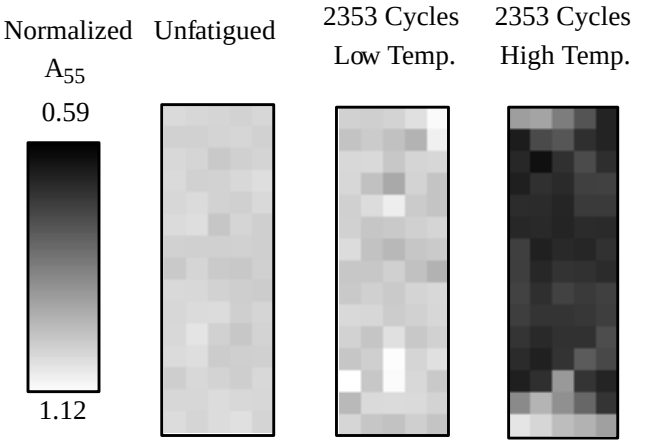

Fig. 7 Stiffness mapping of A_{55} in 75 different regions across the entire panel for samples subjected to TMF at low strain levels

The tabulated values indicate an increase in standard deviation for the samples subjected to TMF as compared to the unfatigued samples. The larger standard deviation in the samples subjected to TMF was most likely due to localized damaged regions in the specimens due to the TMF process. Also, since 5260 is a thermoset, further curing can be occurring in addition to damage accumulation during the initial stages of TMF (Ref 22). The tabulated values also indicate that the standard deviations in the bending stiffnesses, D_{11} and D_{22}, are two to nine times greater than the standard deviations in the out-of-plane shear stiffnesses, A_{55} and A_{44}. As mentioned previously, the inaccuracy in the bending stiffness measurement was due to the lack of data at low frequencies. Due to the inconclusive nature of the bending stiffness data at these TMF levels, the subsequent discussion will concentrate on the out-of-plane stiffness measurements.

The normalized values of A_{55} as a function of cycles for the samples subjected to TMF at low temperatures for both low-strain and high-strain levels are shown in Fig. 9. The results of A_{44} for the same specimens showed a similar trend. Even at extended levels of TMF, the samples showed less than a 10%

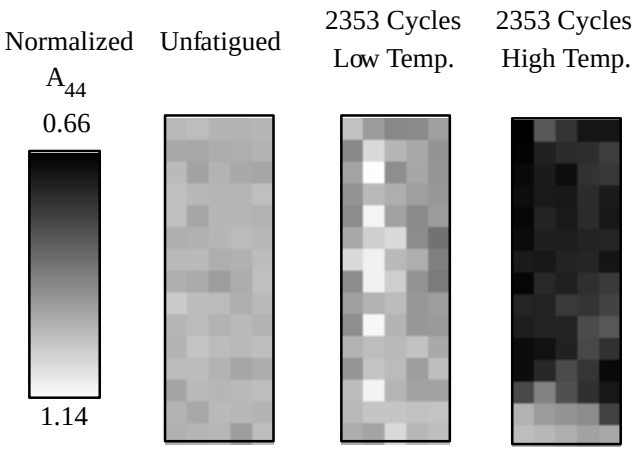

Fig. 8 Stiffness mapping of A_{44} in 75 different regions across the entire panel for samples subjected to TMF at low strain levels

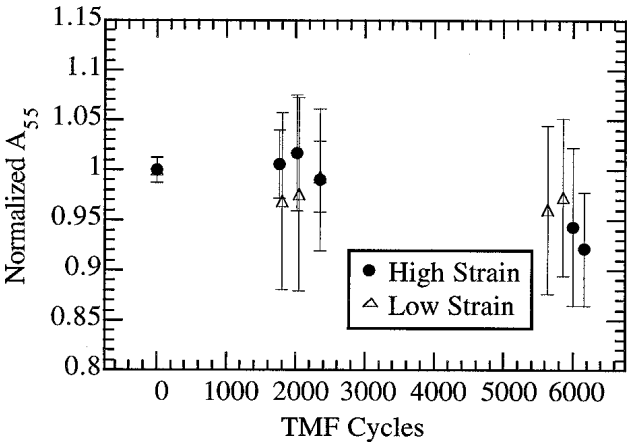

Fig. 9 Normalized A_{55} versus cycles for samples subjected to TMF at low temperatures for low and high strain levels

Table 1 Normalized stiffness measurements for samples subjected to thermal-mechanical fatigue at low strain levels

TMF cycles	Temperature profile	Normalized D_{11}	Normalized A_{55}	Normalized D_{22}	Normalized A_{44}
0	…	1.00 ± 0.09	1.00 ± 0.01	1.00 ± 0.06	1.00 ± 0.02
2353	High	1.01 ± 0.14	0.67 ± 0.04	0.86 ± 0.09	0.73 ± 0.05
4706	High	0.90 ± 0.28	0.36 ± 0.03	0.77 ± 0.16	0.43 ± 0.03
1809	Low	0.92 ± 0.17	0.97 ± 0.09	0.98 ± 0.22	1.01 ± 0.10
2051	Low	0.91 ± 0.18	0.98 ± 0.10	0.97 ± 0.23	1.02 ± 0.10
2353	Low	0.85 ± 0.11	0.99 ± 0.04	1.01 ± 0.21	0.99 ± 0.06
5637	Low	0.93 ± 0.18	0.96 ± 0.08	0.83 ± 0.15	0.96 ± 0.08
5862	Low	0.93 ± 0.15	0.97 ± 0.08	0.82 ± 0.17	0.96 ± 0.09

TMF, thermal-mechanical fatigue

Table 2 Normalized stiffness measurements for samples subjected to thermal-mechanical fatigue at high strain levels

TMF cycles	Temperature profile	Normalized D_{11}	Normalized A_{55}	Normalized D_{22}	Normalized A_{44}
0	…	1.00 ± 0.08	1.00 ± 0.01	1.00 ± 0.06	1.00 ± 0.01
1759	Low	1.01 ± 0.10	1.01 ± 0.03	1.03 ± 0.32	1.01 ± 0.12
2017	Low	1.11 ± 0.16	1.02 ± 0.06	1.07 ± 0.26	1.01 ± 0.07
2353	Low	0.96 ± 0.23	0.99 ± 0.07	1.04 ± 0.29	1.00 ± 0.08
6001	Low	1.03 ± 0.24	0.94 ± 0.08	0.90 ± 0.18	0.90 ± 0.08
6168	Low	1.00 ± 0.18	0.92 ± 0.06	1.03 ± 0.32	0.95 ± 0.10

TMF, thermal-mechanical fatigue

decrease in average stiffness. Shown in Fig. 10 as a function of cycles are the normalized stiffnesses A_{44} and A_{55} for the specimens subjected to TMF at low temperatures and low-strain levels. The stiffnesses for the high-strain profiles showed a similar trend. The average stiffnesses decreased by less than 5% in both the 0 and 90° directions and much larger variations were observed in the thermal-mechanically fatigued samples. Also, there was no discernible difference between the values of A_{44} and A_{55}.

For two samples, a temperature protocol in excess of the recommended maximum operating temperature (135 °C) was used to accelerate the TMF effects. The results for the normalized values of A_{55} for specimens subjected to TMF at low strain levels for high-temperature and low-temperature profiles are shown in Fig. 11. The results of the stiffness A_{44} were similar. In the figure, linear fits to the respective data were made in order to display the difference in trends between the samples. The difference in stiffness loss for the samples subjected to TMF at high temperatures as compared to the ones subjected to TMF at low temperatures was dramatic. Thus, the specimens did not perform well when exposed to temperatures exceeding the recommended levels. This large loss in stiffness was most likely due to oxidative degradation at elevated temperatures.

In addition to the stiffness measurements, time-of-flight scans were conducted on the samples that were removed from the environmental chambers. A four-cycle Gaussian-enveloped sine wave at a fixed frequency of 200 kHz was used to generate the flexural mode, and the received signal was sampled at 25 MHz. The transducers were held fixed at a separation distance of 2.75 cm. The scan area was 73.0 by 24.0 cm in the 0° direction and 73.0 by 22.0 cm in the 90° direction. The step size for all scans was 1.0 cm in each direction. The average time-of-flight for the 0° and 90° scans for samples subjected to low-strain profiles is shown in Table 3. In the table, the values have been normalized to the average time-of-flight obtained for the unfatigued sample.

The tabulated results indicate that the average time-of-flight did not significantly change for the sample subjected to TMF at low temperatures. However, the samples subjected to TMF at high temperatures had an extremely large increase in time-of-flight. The degraded stiffness in these specimens led to a slower Lamb wave velocity, which was reflected by the longer time-of-flight. Also of interest is the increase in standard deviation in the thermal-mechanically fatigued samples as compared to that of the unfatigued sample. This variation is indicative of localized damage regions developing in conjunction with further curing occurring in the samples subjected to TMF (Ref 22). All of these observations are consistent with the stiffness measurements reported earlier.

Shown in Fig. 12 and 13 are the 0° and 90° scans, respectively, for the samples subjected to TMF at low strains and low temperatures. Scans for the samples subjected to TMF to high-temperature extremes are not shown due to the obvious large increase in time-of-flight (see Table 3). In the figures, the values have been normalized to the average time-of-flight for the unfatigued sample. More features were observed in the time-of-flight scans than were seen in the stiffness scans. This was due to the smaller step size used in the time-of-flight scans. Also observed were more features in the samples that were subjected to TMF as compared to the unfatigued sample. This trend is consistent with the increase in variation observed in the stiffness scans for the samples subjected to TMF. Additionally, some features along the ±45° directions were observed in the scans. This was most likely due to matrix cracking along those plies due to TMF.

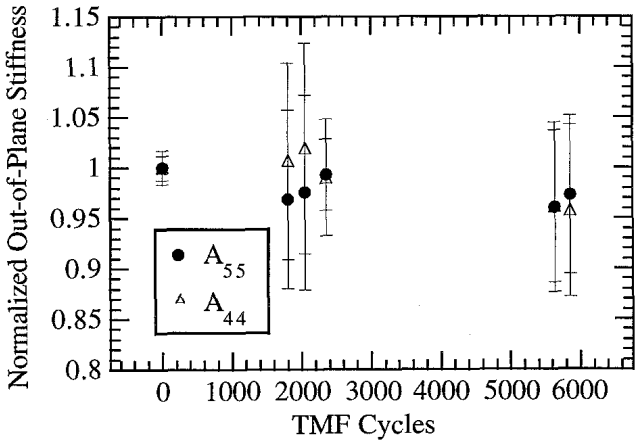

Fig. 10 Normalized A_{44} and A_{55} versus cycles for samples subjected to TMF at low temperatures and low strain levels

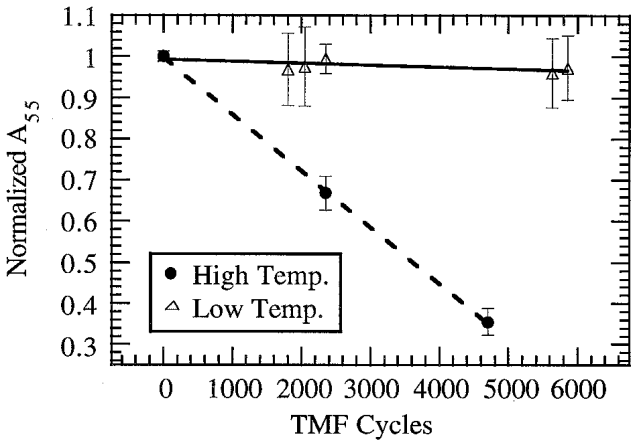

Fig. 11 Normalized A_{55} versus cycles for samples subjected to TMF at low strain levels for high and low temperature profiles. The solid and dashed lines represent linear fits to the respective data.

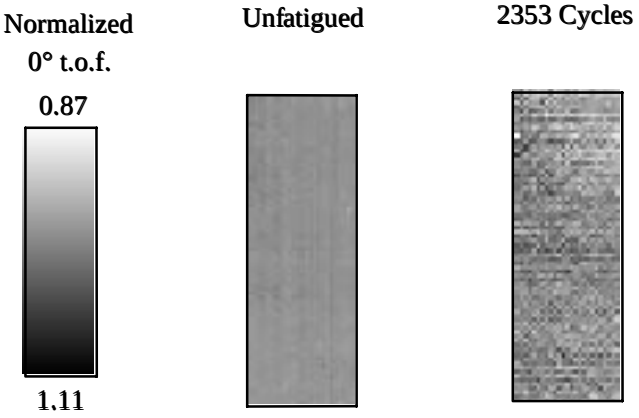

Fig. 12 Normalized time-of-flight (t.o.f.) in the 0° direction in 1800 different regions across the entire panel for samples subjected to TMF at low strains and low temperatures. Step spacing between each scan point was 1.0 cm in each direction.

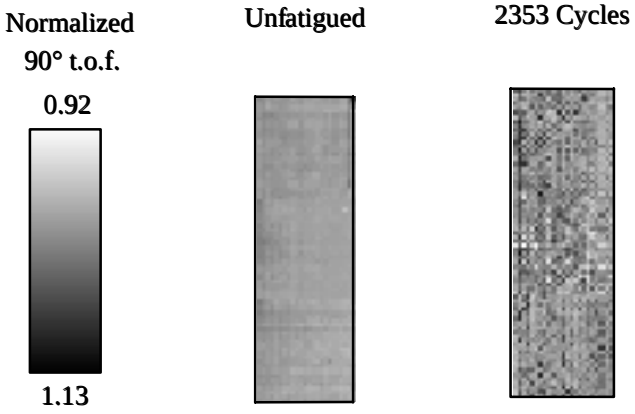

Fig. 13 Normalized time-of-flight (t.o.f.) in the 90° direction in 1656 different regions across the entire panel for samples subjected to TMF at low strains and low temperatures. Step spacing between each scan point was 1.0 cm in each direction.

Table 3 Normalized time-of-flight measurements for samples subjected to thermal-mechanical fatigue at low strain levels

TMF cycles	Temperature profile	Normalized 0° time-of-flight	Normalized 90° time-of-flight
0	…	1.00 ± 0.01	1.00 ± 0.01
2353	Low	1.00 ± 0.03	1.01 ± 0.03
2353	High	1.14 ± 0.03	1.09 ± 0.02
4706	High	1.51 ± 0.06	1.35 ± 0.04

TMF, thermal-mechanical fatigue

6. Conclusions

- Lamb wave imaging has been shown by this study to be a very effective method for providing a quantitative measure of the effects of TMF on composite materials.
- The samples subjected to TMF at low temperatures for both high and low strain levels showed less than a 10% decrease in stiffness after 6168 TMF cycles. However, the samples that were subjected to temperatures in excess of the recommended levels showed a decrease in stiffness of over 60% after 4706 TMF cycles.
- The bending stiffnesses provided inconclusive results due to the large standard deviations in the values.
- Time-of-flight scans showed no change in the average value for the samples subjected to 2353 TMF cycles at low temperatures. However, the average time-of-flight increased by up to 50% for samples subjected to TMF at high temperatures for 4706 cycles.
- All of the samples showed an increased variation in stiffness and time-of-flight for the thermal-mechanically fatigued specimens.

Acknowledgments

This work was performed while Michael D. Seale held a National Research Council NASA-LaRC Research Associateship. The authors thank Steve Ziola, Wei Huang, and John Dorighi of Digital Wave Corporation for their technical support

involving the scanning system. They also thank Karen Whitley of NASA Langley Research Center and Steven Grossen of Lockheed Martin for the micrograph shown in this work.

References

1. T.K. O'Brien, M. Rigamonti, and C. Zanotti, Tension Fatigue Analysis and Life Prediction for Composite Laminates, *Int. J. Fatigue,* Vol 11 (No. 6), 1989, p 379-393
2. A. Charewicz and I.M. Daniel, Damage Mechanisms and Accumulation in Graphite/Epoxy Laminates, *Composite Materials: Fatigue and Fracture,* STP 907, H.T. Hahn, Ed., ASTM, 1986, p 274-297
3. S.L. Ogin, P.A. Smith, and P.W.R. Beaumont, Matrix Cracking and Stiffness Reduction During the Fatigue of a (0/90)s GFRP Laminate, *Compos. Sci. Technol.,* Vol 22, 1985, p 23-31
4. S.L. Ogin, P.A. Smith, and P.W.R. Beaumont, A Stress Intensity Factor Approach to the Fatigue Growth of Transverse Ply Cracks, *Compos. Sci. Technol.,* Vol 24, 1985, p 47-59
5. S.G. Lim and C.S. Hong, Prediction of Transverse Cracking and Stiffness Reduction in Cross-Ply Laminated Composites, *J. Compos. Mater.,* Vol 23, July 1989, p 695-713
6. N. Laws and G.J. Dvorak, Progressive Transverse Cracking in Composite Laminates, *J. Compos. Mater.,* Vol 22, Oct 1988, p 900-916
7. K.N. Street, A.J. Russell and F. Bonsang, Thermal Damage Effects on Delamination Toughness of a Graphite/Epoxy Composite, *Compos. Sci. Technol.,* Vol 32, 1988, p 1-14
8. C.T. Herakovich and M.W. Hyer, Damage-Induced Property Changes in Composites Subjected to Cyclic Thermal Loading, *Eng. Fract. Mech.,* Vol 25, 1986, p 779-791
9. C. Henaff-Gardin, J.L. Desmeuzes, and D. Gaillot, Damage Development Due to Cyclic Thermal Loading in Cross-Ply Carbon/Epoxy Laminates, *Fatigue Under Thermal and Mechanical Loading,* J. Bressers and L. Remy, Ed., Kluwer Academic Publishers, 1996, p 285-293
10. J. Tao, C.T. Sun, C. Arendt, and M. Brunner, Interlaminar Shear Strength and Fracture Behavior in Aged Composite Laminates, *J. Thermoplastic Compos. Mater.,* Vol 11, 1998, p 124-132
11. M.D. Seale, B.T. Smith, and W.H. Prosser, Lamb Wave Assessment of Fatigue and Thermal Damage in Composites, *J. Acoust. Soc. Am.,* Vol 103 (No. 5), Part 1, 1998, p 2416-2424
12. V. Dayal and V.K. Kinra, Ultrasonic NDE of Composites for Transverse Cracking, *Optical Methods in Composites; Proc. of the SEM Fall Conf. on Experimental Mechanics,* (A88-13876 03-24), Society for Experimental Mechanics, Inc., Bethel, CT, 1986, p 17-22
13. B. Tang and E.G. Henneke, II, Lamb-Wave Monitoring of Axial Stiffness Reduction of Laminated Composite Plates, *Mater. Eval.,* Vol 47, 1989, p 928-934
14. V. Dayal, V. Iyer, and V.K. Kinra, Ultrasonic Evaluation of Microcracks in Composites, *Advances in Fracture Research; Proc. of the Seventh International Conf. on Fracture* (ICF7), Vol 5 (A90-41276 18-39), Pergamon Press, New York, 1989, p 3291-3300
15. M.R. Karim, A.K. Mal, and Y. Bar-Cohen, Inversion of Leaky Lamb Wave Data by Simplex Algorithm, *J. Acoust. Soc. Am.,* Vol 88, 1990, p 482-491
16. A.K. Mal, S.-S. Lih, and Y. Bar-Cohen, Ultrasonic Determination of the Elastic Properties Unidirectional Composites, *Review of Progress in Quantitative Nondestructive Evaluation,* Vol 12, D.O. Thompson and D.E. Chimenti, Ed., Plenum Press, New York, 1993, p 1233-1240
17. J.-H. Shih, A.K. Mal, and M. Vemuri, Plate Wave Characterization of Stiffness Degradation in Composites During Fatigue, *Res. Nondestr. Eval.,* Vol 10, 1998, p 147-162
18. Y. Bar-Cohen, S.-S. Lih, A. Mal, and Z. Chang, Rapid Characterization of the Degradation of Composites Using Plate Wave Dispersion Data, *Review of Progress in Quantitative Nondestructive Evaluation,* Vol 17, D.O. Thompson and D.E. Chimenti, Ed., Plenum Press, 1998, p 1171-1176
19. B. Tang, E.G. Henneke II, and R.C. Stiffler, Low Frequency Flexural Wave Propagation in Laminated Composite Plates, *Acousto-Ultrasonics Theory and Application,* John C. Duke, Jr., Ed., Plenum Press, 1987, p 45-65
20. W.H. Prosser, The Propagation Characteristics of the Plate Modes of Acoustic Emission Waves in Thin Aluminum Plates and Thin Graphite/Epoxy Composite Plates and Tubes, *NASA Technical Memorandum 104187,* Nov 1991
21. W. Huang, S.M. Ziola, J.F. Dorighi, and M.R. Gorman, Stiffness Measurement and Defect Detection in Laminated Composites by Dry-Coupled Plate Waves, *Process Control and Sensors for Manufacturing,* R.H. Bossi and D.M. Pepper, Ed., SPIE, Bellingham, WA, 1998, p 66-76
22. W.M. Johnston and T.S. Gates, The Effects of Stress and Temperature on the Open-Hole Tension Fatigue Behavior of a Graphite/Bismaleimide Composite, *Composite Materials: Fatigue and Fracture, Seventh Volume,* STP 1330, R.B. Bucinell, Ed., ASTM, 1998, p 179-198